RSC Advances

ROYAL SOCIETY OF CHEMISTRY

www.rsc.org/advances

RSC Advances

ARTICLE

Biogenic gold nanoparticles-reduced graphene oxide nanohybrid: synthesis, characterization and application in chemical and biological reduction of nitroaromatics

Received 00th January 20xx,
Accepted 00th January 20xx

DOI: 10.1039/x0xx00000x

www.rsc.org/

Bin Dong,[a] Guangfei Liu,[a*] Jiti Zhou,[a] Aijie Wang,[b*] Jing Wang,[a] Ruofei Jin,[a] and Hong Lv[a]

The environment-friendly biosynthesis of gold nanoparticles and reduced graphene oxide nanohybrid (bio-AuNPs/rGO) was achieved with *Shewanella oneidensis* MR-1 under ambient and growing conditions. Both MR-1 cells and its metabolites were vital for the synthesis of bio-AuNPs/rGO, which showed comparable structural features to the chemical synthesized counterpart (chem-AuNPs/rGO). Compared to chem-AuNPs/rGO, bio-AuNPs, bio-rGO and their mixture, bio-AuNPs/rGO not only exhibited better catalytic activity and reusability towards the chemical reduction of 4-nitrophenol, but also showed higher stimulating effect on microbial reduction of nitrobenzene. These might be due to the good morphology/structure properties, introduction of N-doping and synergistic effects between AuNPs and rGO. The MR-1 cells could attach themselves closely to bio-AuNPs/rGO, which might facilitate the transfer of electrons from cells to nitrobenzene during reduction. Moreover, bio-AuNPs/rGO could also enhance the nitrobenzene bioreduction by some MR-1 mutant strains lacking components of the Mtr pathway (*ΔcymA, ΔmtrA* and *ΔmtrB*), whereas no stimulating effect on nitrobenzene reduction by *ΔomcA/ΔmtrC* mutant strain was observed. This study provided a simple and eco-friendly method to synthesize graphene-based nanohybrid capable of stimulating reductive transformation of environmental pollutants.

Introduction

Graphene-based materials have attracted tremendous attention during past years due to their unique physical-chemical properties and potential applications in many fields such as catalysis, biosensor, pollutant removal, energy and so on.[1-4] Decoration of graphene with metal nanoparticles generally resulted in nanohybrid having extraordinary properties.[5-7] Up to now, many approaches have been taken to prepare noble metal/graphene nanohybrid, including chemical reduction in solution, electrochemical deposition, self-assembly between graphene and noble metal nanostructures, and hydrothermal treatment, etc.,[8] among which simultaneous reduction of graphene oxide (GO) and precursor salts of noble metals has been recognized as the most convenient way. To avoid the use of toxic/hazardous strong reductants like hydrazine and $NaBH_4$, environmentally benign and naturally occurring bioreductants such as vitamins and amino acids have been explored for the "green" synthesis of noble metal/graphene nanohybrid.[9] However, prolonged heating (to 95 ℃) was still required in this energy-consuming reducing procedure.

Recently, biosynthesis of nanomaterials such as graphene and metal nanoparticles with microbial cells under ambient and growing conditions has received plenty of attention.[10-13] The dissimilatory metal-reducing bacteria strain *Shewanella oneidensis* MR-1 has been suggested capable of fabricating different kinds of metal nanomaterials[14] and reduced GO (rGO)[10,15] through bioreduction in separate studies. More recently, He et al.[16] have fabricated AuNPs/rGO nanohybrid via a two-step method. They first prepared graphene hydrogels with the help of MR-1 cells. Then the prepared graphene hydrogels were used to adsorb Au(III) ions, which were further reduced to gold nanoparticles due to the reduction potential difference between rGO and $AuCl_4^-$. However, to our knowledge, no information is available for the one-pot biosynthesis of graphene-based nanohybrid using microbial cells and the reaction activity assay of such biogenic nanohybrid.

Nanomaterials were conventionally thought to be detrimental to biological cells and could inhibit biodegradation activity.[17] Graphene-based nanomaterials might decrease bacterial cell viability by direct damage on cell membrane and/or generation of oxidative stress.[18] However, results of recent studies suggested that chemically synthesized graphene and GO can stimulate the bioreduction of nitrobenzene and azo compound by *S. oneidensis* MR-1 and anaerobic sludge,[19,20] respectively. Nanosized carbon materials could not only increase the cell attachment and growth at biomaterials surface, facilitate the extracellular electron transfer through their conductive carbon planes and quinone moieties, but also activate the nitroaromatic molecules with the help of their zigzag edges.[21,22] On the other hand, another study suggested that biogenic gold

[a] Key Laboratory of Industrial Ecology and Environmental Engineering, Ministry of Education, School of Environmental Science and Technology, Dalian University of Technology, Dalian 116024, China. E-mail: guangfeiliu@dlut.edu.cn
[b] State Key Laboratory of Urban Water Resource and Environment, Harbin Institute of Technology, Harbin 150090, China. E-mail: waj0578@hit.edu.cn.
† Electronic Supplementary Information (ESI) available. See
DOI: 10.1039/x0xx00000x

nanoparticles could participate in and repair cell damage in Mtr electron transfer chain of MR-1 to certain extent.[23] More detailed investigations are needed to reveal the ways and mechanisms of graphene and graphene-based nanohybrid interacting with microbial cells during reductive transformation of pollutants.

In this study, we reported for the first time an environmentally benign and one-pot approach to microbially synthesize gold nanoparticles supported on rGO (AuNPs/rGO) through one-pot and simultaneous reduction of GO and $AuCl_4^-$ under culturing conditions. The catalytic performance of biogenic AuNPs/rGO (bio-AuNPs/rGO) towards chemical reduction of 4-nitrophenol (4-NP) was tested and compared with chemically synthesized AuNPs/rGO nanohybrid (chem-AuNPs/rGO). The involvement of biogenic nanomaterials (bio-AuNPs, bio-rGO and bio-AuNPs/rGO) in stimulating electron transfer during bioreductive transformation of nitrobenzene and their interactions with MR-1 cells were also investigated.

Experimental

Chemicals and strains

Graphite powder, $HAuCl_4$, 4-NP, nitrobenzene and all other chemicals were purchased from Sigma-Aldrich or TCI. All of them were of analytical grade and used as received. GO was prepared from graphite powder through modified Hummer's method[24] (see the ESI for details). Chemically synthesized AuNPs/rGO nanohybrid (chem-AuNPs/rGO) was obtained from Nanjing XFNANO Materials Tech Co., Ltd. (Jiangsu, China). According to the information provided by the manufacturer (and also confirmed by our independent characterizations), the weight percentage of Au in chem-AuNPs/rGO was 2% and the mean size of the supported AuNPs was 26.7 nm.

Wild-type *S. oneidensis* MR-1 was purchased from American Typical Culture Center (ATCC 700550). The Δ*cymA*, Δ*mtrA*, Δ*mtrB*, and Δ*omcA*/Δ*mtrC* mutant strains of MR-1 were kindly provided by Prof. Kenneth Nealson from the University of Southern California.[25]

Preparation of bio-AuNPs/rGO nanohybrid

The synthetic route of bio-AuNPs/rGO was shown in Fig. 1. GO dispersion (20 mL, ~1 mg/mL) and $HAuCl_4$ solution (4 mL, 24 mM) were premixed for 2 h. Then the mixture was added into 100 mL of *S. oneidensis* MR-1 culture, which was cultured beforehand for 24 h in Luria–Bertani (LB) broth medium in an incubator shaker (pH ~7, 30 ℃ and 200 rpm). After another 48 h incubation in the shaker, the formed bio-AuNPs/rGO were separated through centrifugation (10,000 *g*, 5 min), soaked in 2.75 M NaOH for 24 h in order to remove the residual bacterial cells and extracellular polymeric substances, washed with ultrapure water until the pH of the supernatant reached neutral, and then kept as aqueous suspension at 4 ℃ before characterization. Bio-AuNPs and bio-rGO were also prepared with MR-1 through the same procedure without the addition of GO or $HAuCl_4$, respectively. To further elucidate the involvement of different components in bio-AuNPs/rGO formation, control experiments were conducted by adding the GO and $HAuCl_4$ mixture into spent medium, MR-1 cell suspension in pure water, and fresh LB medium without inoculation, respectively.

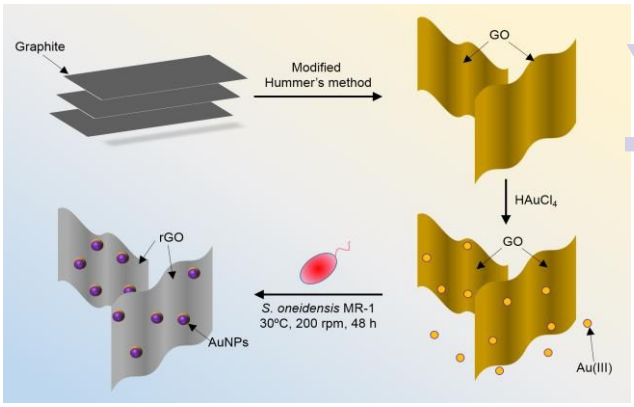

Fig. 1 Illustration of the synthetic route of bio-AuNPs/rGO.

Chemical reduction of 4-NP

The reduction of 4-NP by sodium borohydride ($NaBH_4$) was selected as a model reaction to test the catalytic activity of bio-AuNPs/rGO. In a typical experiment, 20 μL of 4-NP solution (5 mM) and 20 μL of freshly prepared $NaBH_4$ solution (5 M) were added together into a quartz cuvette containing 2 mL of deoxygenized water. Immediately after the addition of bio-AuNPs/rGO suspension (Au, 0.1 mM) and vigorous shaking, the decrease of absorbance of the mixture at 400 nm was monitored using UV-vis spectroscopy (V-560, Jasco Co., Ltd., Japan). The reusability of biogenic AuNPs/rGO as catalyst was tested by repeated addition of 4-NP solution (20 μL, 5 mM) and $NaBH_4$ solution (20 μL, 5 M) into the reaction system after the completion of the former run (no further decrease of absorbance at 400 nm). Totally 10 rounds of reduction were conducted. The catalytic activities of bio-rGO (containing the same rGO mass as that in bio-AuNPs/rGO), bio-AuNPs and chem-AuNPs/rGO (both containing the same Au mass as that in bio-AuNPs/rGO) were also studied.

Enhanced bioreduction of nitrobenzene

The bioreduction of nitrobenzene by *S. oneidensis* MR-1 was studied in modified M-R2A medium.[15] Five-milliliter of overnight MR-1 culture in LB broth medium was harvested through centrifugation, washed twice with sterile phosphate buffer solution (20 mM, pH 7.0), and then resuspended in 40 mL of sterile M-R2A medium in serum bottles, resulting in a biomass concentration of 1.75×10^8 cell/mL. Lactate (18 mM) and nitrobenzene (~200 mg/L) were added as sole electron donor and acceptor, respectively.

To study the impacts of nanomaterials, 50 mg/L bio-AuNPs/rGO and chem-AuNPs/rGO were added into the bioreduction system, respectively. Also, 50 mg/L bio-rGO and 1.5 mg/L bio-AuNPs (containing the same Au mass as that in 50 mg/L bio-AuNPs/rGO) were independently or collectively added into the reduction system to study their effects on nitrobenzene bioreduction. The serum bottles were

anaerobically incubated with shaking at 150 rpm and 30 ℃. Samples were taken at appropriate intervals, filtered through 0.22-μm membrane, and analyzed by high-performance liquid chromatography (HPLC).

Series of MR-1 mutants lacking components of the Mtr pathway (Δ*cymA*, Δ*mtrA*, Δ*mtrB* and Δ*omcA*/Δ*mtrC*) were also tested for nitrobenzene reduction in the absence or presence of bio-AuNPs/rGO.

Enhanced electrochemical reduction of nitrobenzene

The stimulating effects of different nanomaterials on electron transfer and nitrobenzene reduction were further investigated through electrochemical reduction. The modified electrodes were prepared by dropping 10 μL of different suspensions, i.e. 2 mg/mL of bio-AuNPs/rGO, bio-rGO and chem-AuNPs/rGO; and 0.06 mg/L of bio-AuNPs (containing the same Au mass as that in 2 mg/mL bio-AuNPs/rGO) onto the pretreated glass carbon electrodes, which were then dried at room temperature. The electrochemical reactions were carried out in a cell with different modified glass carbon electrodes as working electrodes, Pt gauze electrode (10 × 10 × 0.1 mm) as counter electrode, and Ag/AgCl (3 M KCl) electrode as reference. Cyclic voltammetry measurements were conducted using a CHI 660D electrochemical workstation (CH Instruments, China) in M-R2A medium containing ~200 mg/L of nitrobenzene as electrolyte.

Analytical methods

The prepared bio-AuNPs/rGO was characterized by UV-vis spectroscopy, transmission electron microscopy (TEM), X-ray diffraction (XRD), X-ray photoelectron spectroscopy (XPS), and Fourier transform infrared spectroscopy (FTIR) (see the ESI for details). The concentrations of nitrobenzene and aniline were analyzed by HPLC (Shimadzu LC-20AT, Japan) equipped with an Elite hypersil BDS C18 column (25 μm, 4.6 × 250 mm) for separation at 40 ℃ and a diode array detector (DAD) (SPD-M20A, Japan) for measurement at 254 nm. The mobile phase consisted of 55% methanol and 45% deionized water at a flow rate of 1 mL/min.

Results and discussion

Biosynthesis of AuNPs/rGO nanohybrid

S. oneidensis MR-1 possesses powerful reducing capacity and has been found capable of transforming $AuCl_4^-$ and GO into AuNPs and rGO,[10,14] respectively, providing ways of microbe-mediated simple, green and economical synthesis of high-performance nanomaterials. A premixing of $AuCl_4^-$ and GO for 2 h led to partial adsorption of the $AuCl_4^-$ by GO due to electrostatic or coordinate approaches (Fig. S1). Decreased vibration intensities of O─H (3427 cm^{-1}), C═O (1726 cm^{-1}) and C─O (1056 cm^{-1}) were observed in the FTIR spectra for GO after mixing with $HAuCl_4$ (Fig. S2, line a and b), indicating the interaction between Au(III) and the oxygen-containing groups of GO during adsorption. The maximum adsorption capacity was determined to be 84.3 mg/g, similar to that reported previously.[26] After addition of the mixture, the color of the MR-1 culture gradually changed to black purple (Fig. S3a), indicating the generation of AuNPs-associated products.[14] Through alkaline soak and several rounds of water wash, the products could be well dispersed in water and remained stable for weeks (Fig. S3e). For the FTIR spectrum of bio-AuNPs/rGO (Fig. S2, line c), the infrared peak intensities of oxygen containing groups (O─H, 3400 cm^{-1}, C═O, 1726 cm^{-1} and C─O, 1056 cm^{-1}) further decreased, while that of C═C band (1643 cm^{-1}) substantially increased, indicating the removal of oxygen-containing groups.

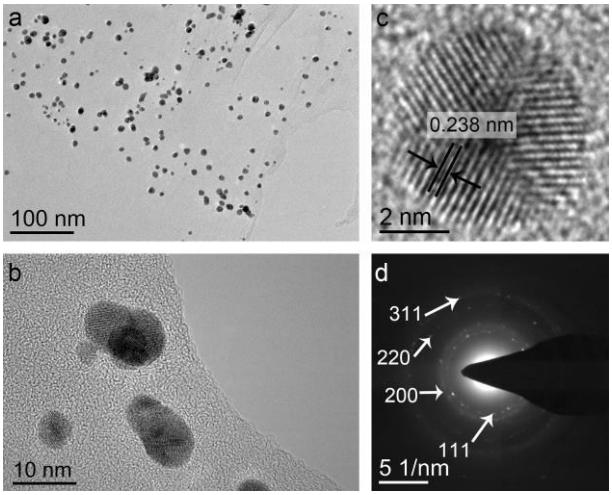

Fig. 2 (a, b) TEM images of bio-AuNPs/rGO, (c) HRTEM micrograph and (d) SAED pattern of the biogenic AuNPs located on rGO.

The UV-vis spectra of GO showed two absorption peaks (Fig. S4), a maximum at 230 nm corresponding to $\pi \rightarrow \pi^*$ transition of aromatic C─C bonds, and a shoulder at 304 nm attributed to $n \rightarrow \pi^*$ transition of C═O bonds.[5] After reduction, the red-shift of peak at 230 nm to 260 nm and the disappearance of the $n \rightarrow \pi^*$ transition band implied the partial restoration of the electronic conjunction within the graphene sheets. Moreover, a new peak at 534 nm was characteristic of the surface plasmon resonance absorption of AuNPs.[5]

TEM analysis indicated that the AuNPs were uniformly anchored on the wrinkled rGO nanosheets (Fig. 2a, b). The diameter of most AuNPs on the rGO sheet was less than 10 nm (mean size = 7.7 ± 2.6 nm) (Fig. S5). The 0.238-nm-spaced fringes detected in the HRTEM image (Fig. 2c) were the 111 lattice fringes of Au. The selected area electron diffraction pattern (Fig. 2d) showed diffraction rings corresponding to (111), (200), (220) and (311) lattice facets of face centered cubic Au (JCPDS 4-0784). EDX analysis revealed the presence of Au, C and O in the nanohybrid (Fig. S6).

XRD analysis was applied to further confirm the formation of bio-AuNPs/rGO nanohybrid (Fig. 3). Diffraction peaks at 38.2 °, 44.4 °, 64.7 ° and 77.8 ° corresponded to the (111), (200), (220) and (311) crystal faces of Au nanoparticles. The average grain size estimated from the Au (111) peak using the Debye Scherrer formula was 7.3 nm, which was in good agreement with the mean particle size observed by TEM analysis. G

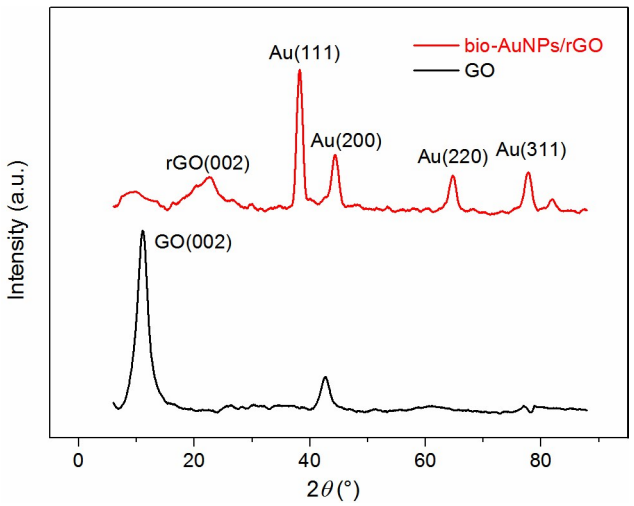

Fig. 3 XRD patterns of bio-AuNPs/rGO and GO.

showed a peak at 11.1 ° corresponding to a d-spacing of 0.79 nm. After reduction, the bio-AuNPs/rGO showed a broad peak centered at around 22.5 ° with a decreasing interlayer spacing of 0.39 nm, which indicated the removal of oxygen-containing groups and the reduction of GO.

XPS was used to identify the surface chemical composition and valence state of GO and bio-AuNPs/rGO. The survey spectrum of GO showed the presence of C 1s and O 1s peaks (Fig. 4a), whereas that of bio-AuNPs/rGO indicated the presence of C 1s, O 1s, N 1s and Au 4f peaks (Fig. 4b). The atomic ratio of carbon and oxygen (C/O) increased from 1.98 of GO to 3.73 of bio-AuNPs/rGO after reaction, indicating the deoxygenation of GO. In the C1s spectra of GO and bio-AuNPs/rGO (Fig. 4c, d), the peak intensities of carbon binding to oxygen decreased dramatically, whereas that of the C─C bond peak increased and became the predominant peak, further indicating the removal of most oxygen-containing functional groups and the restoration of conjugated graphene networks. The negative shift of the peak position of C─C bond from 285.0 eV to 284.8 eV after reduction was ascribed to the different chemical environment of C 1s carbon in bio-AuNPs/rGO. Specifically, the electronegativity of carbon atoms increased due to the removal of oxygen atoms.

The N 1s peak at 400.1 eV (Fig. 4e) corresponded to pyrrolic N, which referred to the N atoms locating in a π conjugated system with two p-electrons.[27] Moreover, the peak at 287.0 eV corresponding to C─O in C 1s spectrum of GO (Fig. 4c) shifted to 286.1 eV in bio-AuNPs/rGO (Fig. 4d), which more likely corresponded to a C─N peak.[28] On the other hand, the N signal was also observed in the FTIR (C─N peak at 1539 cm^{-1}, Fig. S2, line c) and EDX spectra (Fig. S6, inset) of bio-AuNPs/rGO, indicating that N-atoms might be doped into rGO during the microbial synthesis process. The atom ratio of N/C approached 0.18, which was much higher than those of N-doped graphene obtained through GO reduction by mixed microorganisms (0.08)[28] and co-pyrolysis of GO and urea (0.10).[29] The high N content in bio-AuNPs/rGO might be caused by the abundant nitrogen source in LB medium. The Au $4f_{7/2}$ and Au $4f_{5/2}$ peaks appeared at 84.4 and 88.0 eV (Fig. 4f) respectively, again confirming the formation of AuNPs. The positive shift of Au 4f peaks (0.4 eV compared with the characteristic peaks for metallic Au^0 at 84.0 and 87.6 eV) might originate from the withdrawal of valence electron charge by the pyrrole groups and the residual oxygen-containing groups.

Some control experiments were conducted to elucidate the potential mechanism for bio-AuNPs/rGO formation. From the digital pictures and UV-vis spectra (Fig. S3 and S7), it can be seen that similar to the case of incubating GO and $HAuCl_4$ mixture with MR-1 culture, addition of the mixture into MR-1 cells resuspended in pure water and spent medium also resulted in the formation of AuNPs/rGO nanohybrid. For mixture added to MR-1 cells resuspended in pure water, although the reduction products aggregated and settled at the bottom of the glass tube (Fig. S3b), after alkaline wash the resultant product could also form stable AuNPs/rGO aqueous suspension (Fig. S3f). The addition of the mixture into uninnoculated LB medium led to only slightly reduction of $AuCl_4^-$ and no reduction of GO, suggesting the indispensable roles of MR-1 cell and its metabolites for GO reduction. The spent medium was found be capable of reducing GO but not the $AuCl_4^-$ (Fig. S8). Wang et al. also found that spent TSB medium could transform GO to rGO, although at much slower rate than MR-1 culture.[10] The presence of GO, which might provide sites for the nucleation and growth of AuNPs and improve electron transfer,[30] was indispensable for the reduction of $AuCl_4^-$ to AuNPs by fresh LB medium or spent medium (Fig. S8). Moreover, compared to the bio-AuNPs/rGO formed in MR-1 culture, the size and shape distributions of AuNPs in nanohybrid generated by MR-1 suspension in pure water and spent medium were much less homogeneous (Fig. S9).

Catalytic reduction of 4-NP

The time-course of decrease of absorbance at 400 nm for nanomaterials-catalyzed reduction was shown in Fig. 5a. In the absence of catalyst or in the presence of bio-rGO, the peak corresponding to nitrophenolate anion at 400 nm remained unaltered over time. With the addition of bio-AuNPs, bio-AuNPs/rGO or chem-AuNPs/rGO, the absorbance at 400 nm decreased and that of a new peak at 300 nm corresponding to 4-aminophenol increased, indicating the catalytic reduction of 4-NP (Fig. S10). The inset of Fig. 5a showed linear correlations between $\ln(A_t/A_0)$ (A_t and A_0 represent absorbance at 400 nm at time t and zero, respectively) and the reaction time in the presence of different nanomaterials, indicating that the reactions followed pseudo-first-order kinetics. As shown in Table 1, the first-order rate constant normalized by Au molar concentration (k) of bio-AuNPs/rGO was calculated to be 138.45 $s^{-1}M^{-1}$, which was about 10 times higher than that of bio-AuNPs (13.47 $s^{-1}M^{-1}$). In addition, the normalized k values of other nanohybrids of AuNPs and carbon-nanomaterials that were synthesized previously with chemical methods ranged from 1.96 to 33.54 $s^{-1}M^{-1}$, which were also much lower than that of bio-AuNPs/rGO.

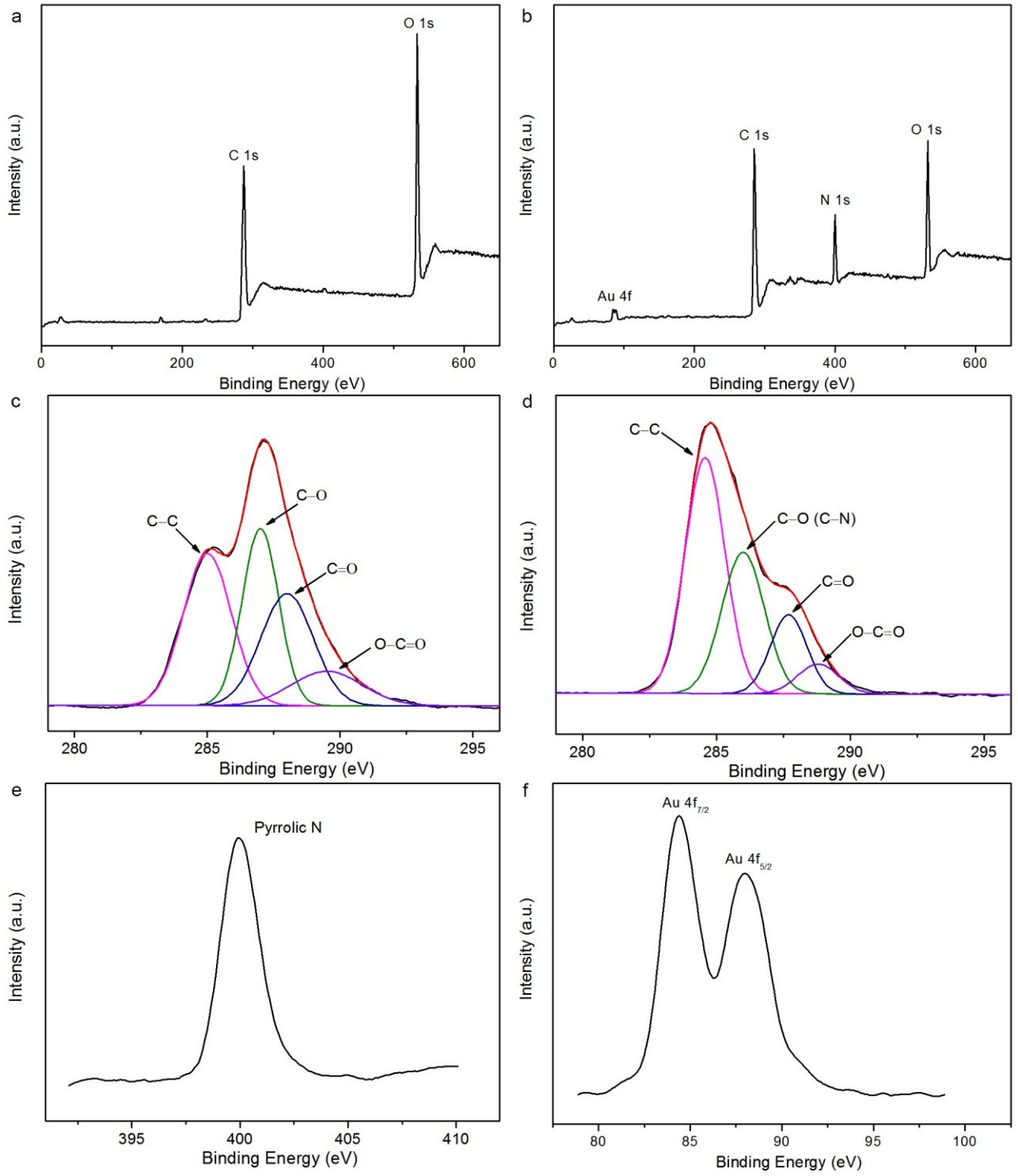

Fig. 4 Survey XPS spectra of (a) GO and (b) bio-AuNPs/rGO; C 1s XPS spectra of (c) GO and (d) bio-AuNPs/rGO; (e) N 1s spectrum and (f) Au 4f spectrum of bio-AuNPs/rGO

Previous studies generally utilized conversion efficiency to demonstrate the reusability of AuNPs-containing catalysts. Although the conversion efficiency of 4-NP could maintain at a high level (>95%) even after running up to eight cycles, the reaction time extended and the catalytic activity decreased significantly when catalysts were used repeatedly.[31] Here, the relative activity factor (k_n/k_1, the subscript represents the cycle number) was used to determine the reusability of catalysts. The catalytic activity of bio-AuNPs/rGO in the tenth round of reduction could still maintain at 72% (Fig. 5b), which was higher than that of G/C–Au (61%) reported previously.[32] However, for chem-AuNPs/rGO and bio-AuNPs, the catalytic

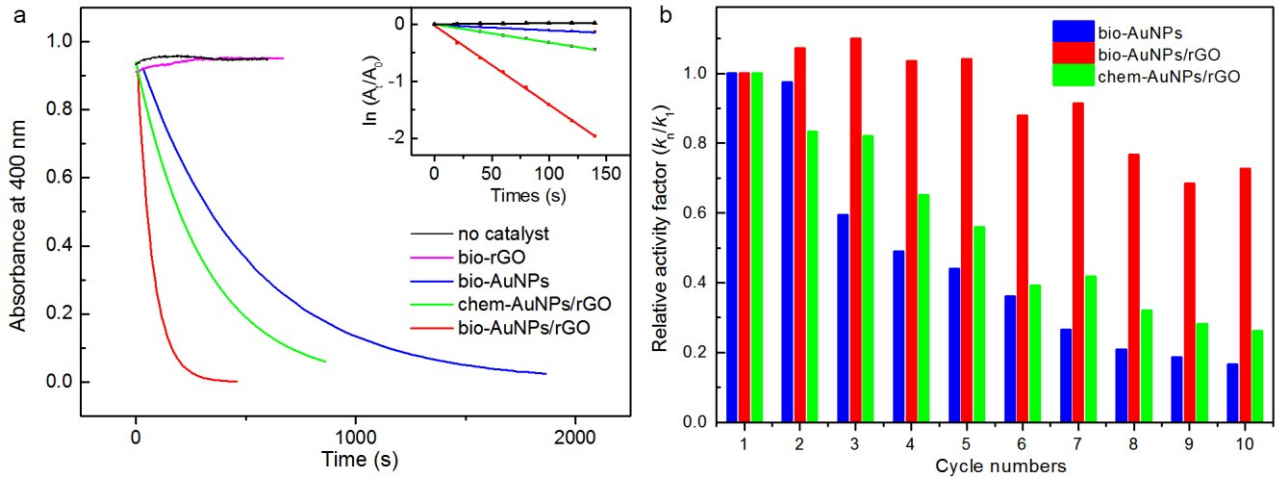

Fig. 5 (a) Plots of absorbance at 400 nm and ln(A/A$_0$) (inset) versus time for the reduction of 4-NP with NaBH$_4$ in the absence of catalyst or in the presence of bio-rGO, bio-AuN bio-AuNPs/rGO and chem-AuNPs/rGO; and (b) the relative activity factors (k_n/k_1, the subscript denotes the cycle number) of bio-AuNPs, bio-AuNPs/rGO and chem-AuNPs/rGO during 10 repeated cycles.

Table 1 Comparison of kinetic constant of 4-NP reduction catalyzed by different nanohybrids of AuNPs and carbon nanomaterials.

Catalysts	Concentrations (mM)			k ($s^{-1}M^{-1}$)	Refs
	4-NP	NaBH$_4$	Au		
bio-AuNPs/rGO	0.05	50	0.10	138.45	this study
bio-AuNPs	0.05	50	0.10	13.47	this study
chem-AuNPs/rGO	0.05	50	0.10	31.99	this study
G/C-Au	25	2500	0.31	18.27	ref. 32
AuNPs/rGO	0.1	67	0.10	31.30	ref. 5
AuNPs/TWEEN/GO	3.5	80	2.16	1.96	ref. 33
AuNPs/GO	3.5	80	0.23	13.75	ref. 34
Au@PZS@CNTs	0.1	5	0.05	33.54	ref. 35

activity decreased rapidly from the second and third cycle, respectively. Almost no morphology change was observed with bio-AuNPs/rGO after ten rounds of repeated reduction (Fig. S11). The excellent catalytic performance and high reusability of bio-AuNPs/rGO might arise from the synergistic effects of AuNPs and rGO. The rGO support inhibits the significant aggregation of AuNPs. Its high adsorption capacity increased the 4-NP concentration near the AuNPs on rGO and led to efficient contacts between them. Also, the conductive rGO could accelerate the electron transfer and facilitate the uptake of electrons by 4-NP molecules.[5]

Bioreduction of nitrobenzene

It has been suggested that chemically synthesized carbon nanomaterials could stimulate the bioreduction of nitrobenzene.[19] Here, the effects of biogenic nanomaterials on nitrobenzene reduction by *S. oneidensis* MR-1 were studied. As shown in Fig. 6, no obvious difference in reduction efficiency was found among systems added with different nanomaterials in the first 12 h, during which time contacts between cells and nanomaterials to form complex might occur. After that, system added with bio-AuNPs/rGO gradually demonstrated its advantage in reduction efficiency over system containing MR-1 alone. In 48 h, the nitrobenzene reduction efficiency was greatly increased from 41% to 67% in the presence of bio-AuNPs/rGO. Moreover, although to some less extents, stimulating effects were also observed with systems added with other nanomaterials. In 120 h, over 75% reduction of nitrobenzene was observed in systems supplemented with bio-AuNPs/rGO and bio-rGO, and around 60% reduction was obtained in systems added with other nanomaterials, all of which were higher than that (53%) of system containing only MR-1 cell. The nitrobenzene bioreduction rates obtained here were comparable to those reported previously (Table S1). It should be noted that the reduction rate obtained in the presence of bio-AuNPs/rGO was even higher than those reported previously in systems containing 2.9-4.1 times more biomass. Interestingly, mixture of bio-AuNPs and bio-rGO (with the same mass and content as those of bio-AuNPs/rGO) could not achieve the same stimulating effects of bio-AuNPs/rGO, suggesting the importance of synergistic effects in bio-AuNPs/rGO nanohybrid. Similar to results of chemical reduction of 4-NP, the stimulating effect of chem-AuNPs/rGO was much poorer than that of bio-AuNPs/rGO.

As shown in Fig. 7a and b, MR-1 cells attached themselves closely to the bio-AuNPs/rGO sheets and had direct contacts with both rGO and AuNPs, which could facilitate the transfer and extend the reach of biogenerated electrons. We also found

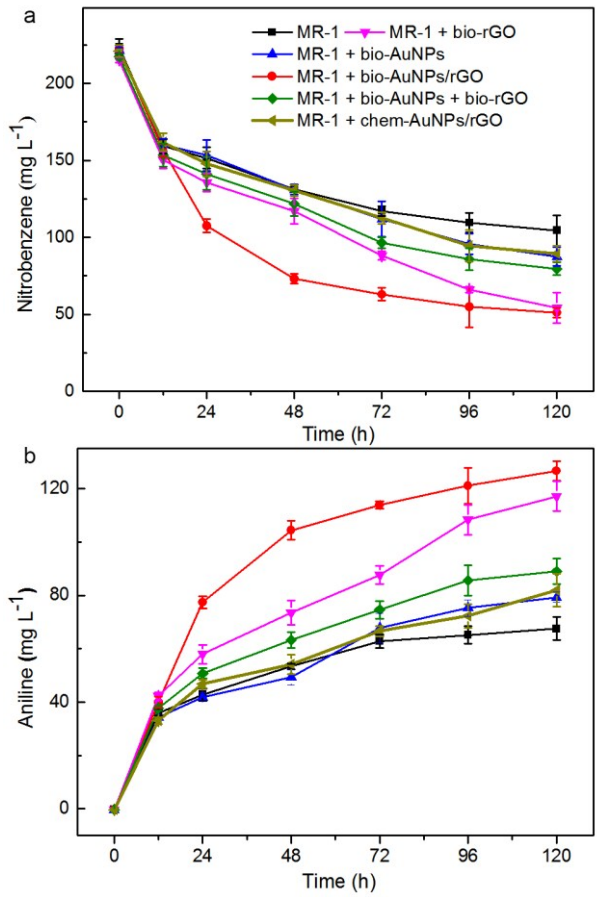

Fig. 6 The changes of (a) nitrobenzene and (b) aniline concentrations during nitrobenzene bioreduction by *S. oneidensis* MR-1 in the absence or presence of different nanomaterials.

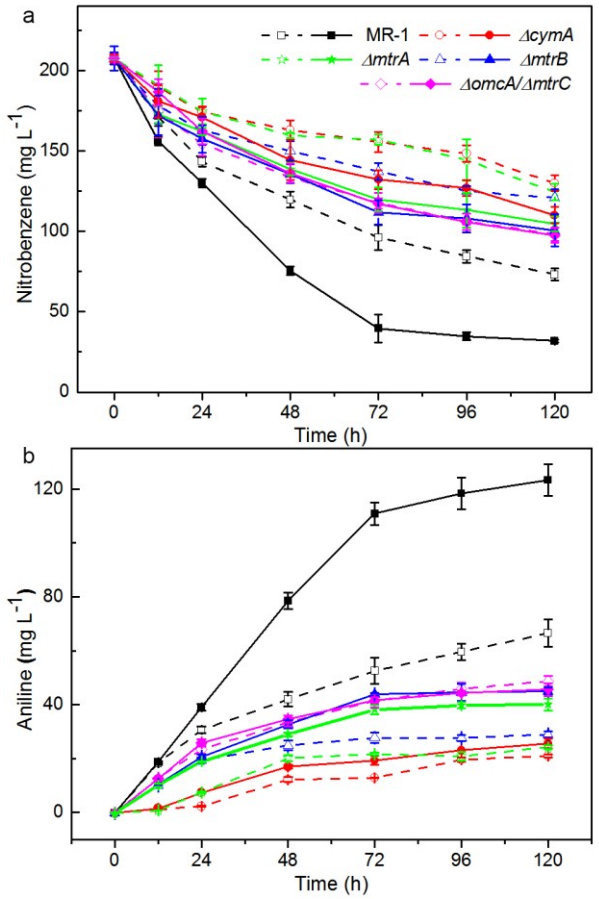

Fig. 8 The changes of (a) nitrobenzene and (b) aniline concentrations during nitrobenzene bioreduction by *S. oneidensis* MR-1 wild-type and mutant strains in the absence (dash) or presence (solid) of bio-AuNPs/rGO.

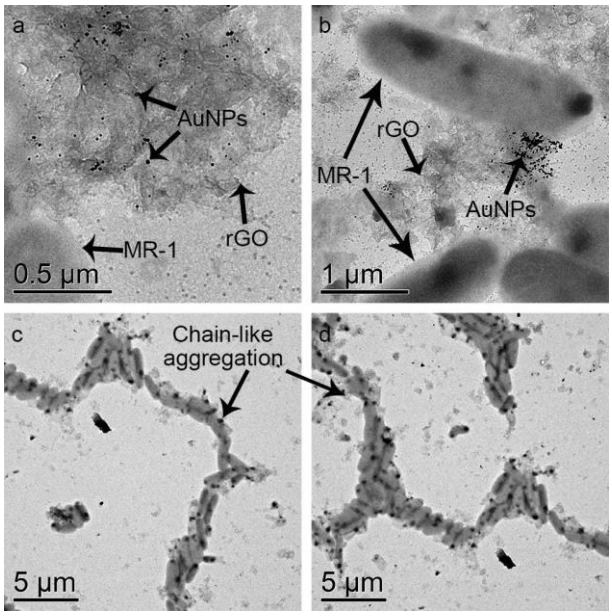

Fig. 7 (a, b) *S. oneidensis* MR-1 cells attached themselves closely to the bio-AuNPs/rGO sheets. (c, d) Chain-like aggregates formed by *S. oneidensis* MR-1 and bio-AuNPs/rGO.

that, in some cases, the MR-1 cells and bio-AuNPs/rGO could form chain-like aggregates together at a length of 30-40 μm (Fig. 7c, d). This unique aggregate might help the translocation, exchange and long-distance transfer of electrons between cells, and thus improve their metabolism activities.

The cyclic voltammetry measurement conducted in M-R2A medium containing nitrobenzene (~200 mg/L) showed that electrode-modified with bio-AuNPs/rGO had a substantially higher specific capacitance and much higher electrochemical activity towards the electrical reduction of nitrobenzene (Fig. S12). The cathodic peak at -0.80 V (peak a) was attributed to the reduction of nitrobenzene to phenylhydroxylamine. The anodic peak at -0.10 V (peak b) and the cathodic peak at -0.20 V (peak c, only observed from the second cycle) were a pair of redox peaks of phenylhydroxylamine and nitrosobenzene.[36] Other nanomaterials could also enhance the electrochemical reduction of nitrobenzene in a descending order of bio-AuNPs/rGO>bio-rGO>chem-AuNPs/rGO>bio-AuNPs, which was similar to that obtained for bioreduction experiments, and indicated again that bio-AuNPs/rGO was more efficient in the electron transfer from donor (electrode or cell) to acceptor (nitrobenzene).

Mutant strains were utilized to further clarify the pathway MR-1 employed for nitrobenzene reduction in the absence or presence of bio-AuNPs/rGO. Unlike a previous report indicating that components of the Mtr respiratory pathway other than CymA were not involved in nitrobenzene reduction,[37] we observed decreased reduction performance of mutants lacking any component of Mtr pathway (Fig. 8). This disagreement might be caused by the use of different cell concentrations. The biomass used by Cai et al.[37] was 5×10^8 cell/mL, which was 2.9 times higher than that applied in this study. When we repeated the experiments of Cai et al. by increasing the cell concentration to 5×10^8 cells/mL, no obvious difference in nitrobenzene reduction was observed between wild type MR-1 and its mutants including Δ*mtrA*, Δ*mtrB* and Δ*omcA*/Δ*mtrC* (Fig. S13). Potential periplasmic nitroreductase or other electron transfer modules parallel to Mtr might be responsible for the remaining nitrobenzene reduction activity of mutants.[37] And the presence of excess biomass of mutant strains could cover up the deficiencies of Mtr mutant strains in nitrobenzene reduction.

Besides improving nitrobenzene reduction by the wild-type MR-1, the presence of bio-AuNPs/rGO could also significantly stimulate the nitrobenzene reduction by Δ*cymA*, Δ*mtrA* and Δ*mtrB* mutant strains (Fig. 8 and Fig. S14). In 120 h, with the addition of bio-AuNPs/rGO, the nitrobenzene reduction efficiency of wild-type MR-1 was increased by 20%, whereas those of the three mutants were increased by around 10%. (Semi)conductive magnetite nanoparticle has also been suggested to compensate for the lack of pilin-associated cytochrome *c* in extracellular electron exchange.[38] In contrast, no improvement in nitrobenzene reduction was observed with the Δ*omcA/*Δ*mtrC* mutant strain in the presence of bio-AuNPs/rGO. These two *c*-type cytochromes that located on the outer membrane and extended as structural components of MR-1's nanowires have been well recognized for participating in and facilitating extracellular electron transfer.[39] From our results it can be seen that OmcA and MtrC are vital for the utilization of bio-AuNPs/rGO to improve nitrobenzene reduction. Similarly, Yan et al.[19] also found that OmcA and MtrC are important for MR-1 to utilize carbon nanotube immobilized together with cells in alginate beads to speed up nitrobenzene reduction. Based on results of electrochemistry studies with cytochrome *c* and nanomaterials,[40,41] we deduced that the conductive and nano-sized bio-AuNPs/rGO used here might get close contact and cooperate with these two *c*-type cytochromes to accelerate the reduction of nitrobenzene. The Mtr pathway well-known for extracellular electron transfer also plays an important role in both direct and nanomaterials-mediated reduction of nitrobenzene.

Conclusions

AuNPs/rGO nanohybrid was successfully fabricated with microbial cells for the first time. The resultant bio-AuNPs/rGO showed good morphology/structure characteristics. The catalytic activity and reusability of bio-AuNPs/rGO towards the chemical reduction of 4-NP exceeded those of many chemically synthesized nanohybrids of AuNPs and carbon nanomaterials. In addition, the bio-AuNPs/rGO could contact closely with *S. oneidensis* MR-1 cells and efficiently enhance nitrobenzene bioreduction by wild-type and mutant strains. The *c*-type cytochromes of Mtr pathway could cooperate with nanomaterials in enhancing electron transfer to nitrobenzene. The biological synthesis approach developed here for graphene-based nanohybrid avoids the use of toxic/hazardous chemicals and harsh conditions. And the biogenic nanohybrid could be applied to improve the chemical and microbial reduction of environmental pollutants.

Acknowledgements

We thank the Natural Science Foundation of China (No. 51478076) and Open Project of State Key Laboratory of Urban Water Resource and Environment, Harbin Institute of Technology (No. QAK201530) for partial support of this study.

References

1. C. Xu, X. Wang and J. Zhu, *J. Phys. Chem. C*, 2008, **112**, 19841-19845.
2. L. Zeng, R. Wang, L. Zhu and J. Zhang, *Colloids Surf. B: Biointerfaces*, 2013, **110**, 8-14.
3. S. Wang, H. Sun, H. M. Ang and M. Tadé, *Chem. Eng. J.*, 2013, **226**, 336-347.
4. X. Li, H. Zhu, K. Wang, A. Cao, J. Wei, C. Li, Y. Jia, Z. Li, X. Li and D. Wu, *Adv. Mater.*, 2010, **22**, 2743-2748.
5. J. Li, C. Liu and Y. Liu, *J. Mater. Chem.*, 2012, **22**, 8426-8430.
6. T. Qian, C. Yu, S. Wu and J. Shen, *Colloids Surf. B: Biointerfaces*, 2013, **112**, 310-314.
7. H. Li, S. Liu, J. Tian, L. Wang, W. Lu, Y. Luo, A. M. Asiri, A. O. Al-Youbi and X. Sun, *ChemCatChem*, 2012, **4**, 1079-1083.
8. C. Zhu and S. Dong, *Nanoscale*, 2013, **5**, 10765-10775.
9. M. Fernández-Merino, S. Villar-Rodil, J. Paredes, P. Solís-Fernández, L. Guardia, R. García, A. Martínez-Alonso and J. Tascón, *Carbon*, 2013, **63**, 30-44.
10. G. Wang, F. Qian, C. W. Saltikov, Y. Jiao and Y. Li, *Nano Res.*, 2011, **4**, 563-570.
11. S. Gurunathan, J. W. Han, V. Eppakayala and J. H. Kim, *Colloids Surf. B: Biointerfaces*, 2013, **102**, 772-777.
12. N. I. Hulkoti and T. C. Taranath, *Colloids Surf. B: Biointerfaces*, 2014, **121**, 474-483.
13. K. Kalishwaralal, V. Deepak, S. R. K. Pandian, M. Kottaisamy, S. BarathmaniKanth, B. Kartikeyan and S. Gurunathan, *Colloids Surf. B: Biointerfaces*, 2010, **77**, 257-262.
14. A. K. Suresh, D. A. Pelletier, W. Wang, M. L. Broich, J. W. Moon, B. Gu, D. P. Allison, D. C. Joy, T. J. Phelps and M. J. Doktycz, *Acta Biomater.*, 2011, **7**, 2148-2152.
15. G. Liu, X. Zhang, J. Zhou, A. Wang, J. Wang, R. Jin and H. Lv, *Bioresour. Technol.*, 2013, **149**, 503-508.
16. Y. He, Y. Cheng, W. Wang and H. Yu, *Chem. Eng. J.*, 2015, **270**, 476-484.
17. J. Zhao, Z. Wang, J. C. White and B. Xing, *Environ. Sci. Technol.*, 2014, **48**, 9995-10009.
18. A. M. Pinto, I. C. Goncalves and F. D. Magalhaes, *Colloids Surf. B: Biointerfaces*, 2013, **111**, 188-202.
19. F. Yan, Y. He, C. Wu, Y. Cheng, W. Li and H. Yu, *Environ. Sci. Technol. Lett.*, 2014, **1**, 128-132.
20. J. Wang, D. Wang, G. Liu, R. Jin and H. Lv, *J. Chem. Technol. Biotechnol.*, 2014, **89**, 750-755.

21. H. Fu and D. Zhu, *Environ. Sci. Technol.*, 2013, **47**, 4204-4210.
22. S. Y. Oh, J. G. Son and P. C. Chiu, *Environ. Earth Sci.*, 2015, **73**, 1813-1822.
23. R. Wu, L. Cui, L. Chen, C. Wang, C. Cao, G. Sheng, H. Yu and F. Zhao, *Sci. Rep.*, 2013, **3**, 3307.
24. W. S. Hummers Jr and R. E. Offeman, *J. Am. Chem. Soc.*, 1958, **80**, 1339-1339.
25. O. Bretschger, A. Obraztsova, C. A. Sturm, I. S. Chang, Y. A. Gorby, S. B. Reed, D. E. Culley, C. L. Reardon, S. Barua and M. F. Romine, *Appl. Environ. Microbiol.*, 2007, **73**, 7003-7012.
26. L. Liu, S. Liu, Q. Zhang, C. Li, C. Bao, X. Liu and P. Xiao, *J. Chem. Eng. Data*, 2013, **58**, 209-216.
27. D. Wei, Y. Liu, Y. Wang, H. Zhang, L. Huang and G. Yu, *Nano Lett.*, 2009, **9**, 1752-1758.
28. M. Fan, C. Zhu, Z. Feng, J. Yang, L. Liu and D. Sun, *Nanoscale*, 2014, **6**, 4882-4888.
29. H. Zhao, W. Wang, Q. Lv, T. Lin, Q. Lin and H. Yang, *Bioresour. Technol.*, 2015, **176**, 106-111.
30. G. Goncalves, P. A. Marques, C. M. Granadeiro, H. I. Nogueira, M. Singh and J. Gracio, *Chem. Mater.*, 2009, **21**, 4796-4802.
31. Y. Zhu, J. Shen, K. Zhou, C. Chen, X. Yang and C. Li, *J. Phys. Chem. C*, 2010, **115**, 1614-1619.
32. F. Yang, C. Wang, L. Wang, C. Liu, A. Feng, X. Liu, C. Chi, X. Jia, L. Zhang and Y. Li, *RSC Adv.*, 2015, **5**, 37710-37715.
33. W. Lu, R. Ning, X. Qin, Y. Zhang, G. Chang, S. Liu, Y. Luo and X. Sun, *J. Hazard. Mater.*, 2011, **197**, 320-326.
34. Y. Zhang, S. Liu, W. Lu, L. Wang, J. Tian and X. Sun, *Catal. Sci. Technol.*, 2011, **1**, 1142.
35. X. Wang, J. Fu, M. Wang, Y. Wang, Z. Chen, J. Zhang, J. Chen and Q. Xu, *J. Mater. Sci.*, 2014, **49**, 5056-5065.
36. Y. Li, H. Cao, C. Liu and Y. Zhang, *J. Hazard. Mater.*, 2007, **148**, 158-163.
37. P. Cai, X. Xiao, Y. He, W. Li, L. Yu, M. H. W. Lam and H. Yu, *Biochem. Eng. J.*, 2012, **68**, 227-230.
38. F. Liu, A. E. Rotaru, P. M. Shrestha, N. S. Malvankar, K. P. Nevin and D. R. Lovley, *Environ. Microbiol.*, 2015, **17**, 648-655.
39. S. Pirbadian, S. E. Barchinger, K. M. Leung, H. S. Byun, Y. Jangir, R. A. Bouhenni, S. B. Reed, M. F. Romine, D. A. Saffarini and L. Shi, *Proc. Natl. Acad. Sci.*, 2014, **111**, 12883-12888.
40. J. Wu, M. Xu and G. Zhao, *Electrochem. Commun.*, 2010, **12**, 175-177.
41. K. Caban, A. Offenhäusser and D. Mayer, *Phys. Status Solidi A*, 2009, **206**, 489-500.

Table of contents entry

The biogenic AuNPs/rGO can participate in and accelerate electron transfer, and catalyze both chemical and biological reduction of nitroaromatics efficiently.